Self-Assembly Structures through Competitive Interactions of Crystalline−Amorphous Diblock Copolymer/Homopolymer Blends: Poly(ε-caprolactone-*b*-4-vinyl pyridine)/Poly(vinyl phenol)

Wan-Chun Chen,[†] Shiao-Wei Kuo,*[,‡] Chu-Hua Lu,[†] U-Ser Jeng,[§] and Feng-Chih Chang*[,†]

Institute of Applied Chemistry, National Chiao Tung University, Hsin Chu, Taiwan, Department of Materials and Optoelectronic Science, Center for Nanoscience and Nanotechnology, National Sun Yat-Sen University, Kaohsiung, Taiwan, and National Synchrotron Radiation Research Center, Hsinchu Science Park, Taiwan

Received October 31, 2008

ABSTRACT: A series of immiscible crystalline−amorphous diblock copolymers, poly(ε-caprolactone)-*b*-(4-vinyl pyridine) (PCL-*b*-P4VP), were synthesized through combination of sequential ring-opening and controlled living free radical (nitroxide-mediated) polymerizations and then blended with poly(vinyl phenol) (PVPh) homopolymer. Miscibility and self-assembly morphologies mediated by hydrogen-bonding interactions of this new A−B/C type polymer blend are discussed in detail. Self-assembly morphologies of these immiscible PCL-*b*-P4VP diblock copolymers change through competitive hydrogen-bonding interactions with the increase of PVPh contents The SAXS profiles also reveal a sharp primary peak and highly long-range order reflections such as cylinder or sphere structure at relatively lower PVPh content, which is consistent with TEM images. DSC, WAXD, and FT-IR analyses provide positive evidence that the pyridine group of P4VP is a significantly stronger hydrogen-bond acceptor than the carbonyl group of PCL with the hydroxyl group of PVPh and results in the excluded and confined PCL phase.

Introduction

Self-organizing materials make the "bottom up" method a relative simple and low-cost process to fabricate large-area periodic nanostructures from diblock copolymers by controlling their self-assembly behavior. Diblock copolymers can form many different well-defined self-assembled nanostructures in the bulk state, including lamellar, hexagonally packed cylindrical, and body-centered cubic micellar structures, as a result of the presence of two immiscible polymer chains connected by covalent bonds and depending on the relative volume fractions of the blocks, the total degree of polymerization, and Flory−Huggins interaction parameter.[1−4]

In addition, blending diblock (A-*b*-B) copolymers with homopolymers have attracted much interest in polymer science during the past few years because of the unusual phase behavior of such systems.[5−11] Most studies have concentrated on blending an immiscible A-*b*-B diblock copolymer with a homopolymer A. Another major system that has been investigated is the blending of a homopolymer C with an immiscible A-*b*-B diblock copolymer, where C is immiscible with block A but interacts favorably with block B. Zhao et al. first investigated the blending of immiscible poly(styrene-*b*-vinyl phenol) (PS-*b*-PVPh) diblock copolymers with various hydrogen-bond acceptor polymers, such as poly(ethylene oxide) (PEO), poly(4-vinyl pyridine) (P4VP), and poly(butyl methacrylate) (PBMA), which can form hydrogen bonds with PVPh, yet are immiscible with the PS block.[6] Ikkala et al. reported the blending of the immiscible polyisoprene-*b*-poly(2-vinyl pyridine) (PI-*b*-P2VP) diblock copolymer with novolac resin. The hydrogen-bonding interactions between the hydroxyl groups of novolac with the pyridine groups of P2VP can result in a miscible phase, even though novolac is immiscible with PI. As a result, a separate glass transition temperature can be observed for the PI block.[12] Recently, Matsushita et al. also reported the blending of immiscible polystyrene-*b*-poly(2-vinyl pyridine) (PS-*b*-P2VP) with PVPh homopolymer, and only the microphase separation was observed with blending with PVPh, even upon addition of a large amount of PVPh, which is in contrast with the addition of P2VP homopolymer.[11]

Several systems comprising an immiscible A-*b*-B diblock copolymer and a homopolymer C, where C is miscible with both A and B, have been reported. For example, Kwei et al. investigated blends of poly(styrene-*b*-vinyl phenol)/poly(vinyl methyl ether) (PS-*b*-PVPh/PVME), where PVME is miscible with both PS and PVPh blocks and serves as a common solvent; this system results in a single phase when the PVME content is higher than 50 wt %.[6] Guo et al. reported an immiscible A-*b*-B diblock copolymer, where C is miscible with both blocks A and B, but the hydrogen-bonding interactions between the B and C segments are stronger than those of the A and C segments ($\chi_{BC} \gg \chi_{AC}$). They investigated the selective hydrogen bonding in poly(ε-caprolactone)-*b*-poly(2-vinyl pyridine) (PCL-*b*-P2VP) with phenoxy resin and poly(vinyl phenol) (PVPh), where both of the blocks are miscible with the phenoxy resin and PVPh and the value of χ_{AB} is positive (A and B are immiscible), and χ_{AC} and χ_{BC} are negative, but χ_{BC} is more negative than χ_{AC}.[13,14] The selective hydrogen-bonding interaction leads to the formation of a variety of composition-dependent microphase separations. However, the detailed phase diagram and specific competitive interactions were not reported due to only one composition in diblock copolymer in the above cases.

On the basis of those reasons, we would like to synthesize a series of poly(ε-caprolactone)-*b*-poly(4-vinyl pyridine) (PCL-*b*-P4VP) diblock copolymers through combinations of ring-opening polymerization (ROP) of ε-caprolactone (ε-CL) followed by nitroxide-mediated radical polymerization (TEMPO) of 4-vinylpyridine (4-VP) and then blending with PVPh. We

* To whom correspondence should be addressed. (F.-C.C.) Telephone: Fax: 886-3-5131512. E-mail: changfc@mail.nctu.edu.tw. (S.-W.K.) E-mail: kuosw@faculty.nsysu.edu.tw. Fax: 886-7-525 4099.
[†] National Chiao Tung University.
[‡] National Sun Yat-Sen University.
[§] National Synchrotron Radiation Research Center.

10.1021/ma900080v CCC: $40.75
Published on Web 05/01/2009

Scheme 1. Synthetic Routes of (a) Radical Addition among Benzoyolxyl Radicals, Styrene, and 4-OH TEMPO, and (b) Ring-Opening Polymerization of ε-CL and Nitroxide-Mediated Radical Polymerization of 4-VP after Reaction between Hydroxyl-4-oxo-*N*-alkoxyamines and Triethyl Aluminum

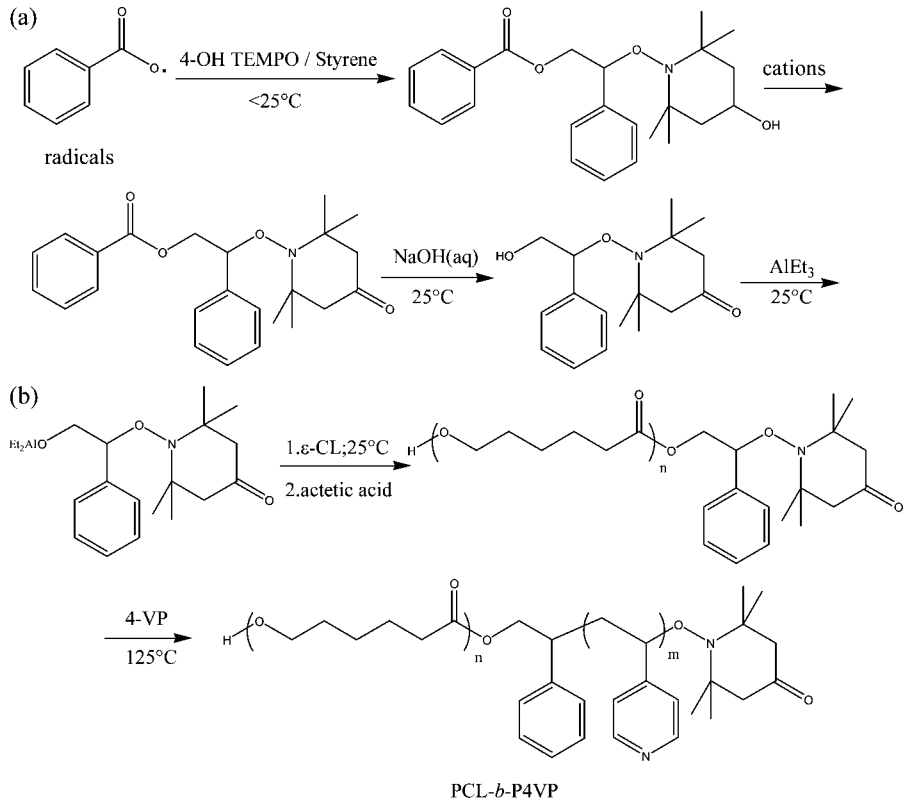

have investigated that the hydrogen-bonding interaction of the miscible PVPh/P4VP blend ($K_A = 598$)[15] is much stronger than that of the miscible PVPh/PCL blend ($K_A = 90$)[16,17] based on the Painter−Coleman association model,[18,19] where the PCL/P4VP blend is immiscible. The phase diagrams and competitive specific interactions were characterized by DSC, WAXD, TEM, SAXS, and FT-IR in this study.

Experimental Section

Materials. Poly(vinyl phenol) (PVPh) used in this study was prepared by living anionic polymerization of 4-*tert*-butoxystyrene, and then the *tert*-butoxy protective group was selectively removed through subsequent hydrolysis reaction. Various PCL-*b*-P4VP copolymers studied in this work are sequentially synthesized by ring-opening polymerization (ROP) of ε-caprolactone followed by free radical polymerization of 4-vinylpyridine as described in Scheme 1. The detailed synthetic route and characterizations of the synthesized copolymers were described elsewhere.[20−24]

Blend Preparation. Blending samples of various weight percents of PCL-*b*-P4VP/PVPh compositions were prepared through solution casting. DMF solution containing 5 wt % polymer mixture was stirred for 8−10 h and then cast on a Teflon dish. The solution was left to evaporate slowly at 80 °C for 1 day and then dried under a vacuum oven at 120 °C for 14 days.

Characterizations. Thermal analysis was carried out using a DSC instrument (TA Instruments Q-20). The sample (ca. 4−6 mg) was weighed and sealed in an aluminum pan. For nonisothermal crystallization experiments, the samples were first annealed at 210 °C for 10 min and then cooled at −90 at 5 °C/min for recording the crystallization exotherm. The temperature corresponding to the exothermic peak was denoted as T_f. The glass transition temperature (T_g) was taken as the midpoint of the heat capacity transition between the upper and lower points of deviation from the extrapolated glass and liquid lines with a scan rate of 20 °C/min and a temperature range of −90 to 250 °C. TEM analysis was performed using a Hitachi H-7100 electron microscope operated at 100 kV. Ultrathin sections of the samples were prepared using a Leica Ultracut S microtome equipped with a diamond knife. Slices of ca. 700 Å thickness were cut at −120 °C. The ultrathin sections were picked onto the copper grids coated with carbon-supporting films followed by staining by exposure to the vapor of 4% RuO_4 aqueous solution for 25 min. Because RuO_4 is a preferential staining agent, P4VP, PVPh, and P4VP/PVPh domains appear dark, and the PCL domain appears bright in the micrographs, respectively. Wide-angle X-ray diffraction (WAXD) measurements were carried out using a Bruker Nanostar U System, with an incident X-ray wavelength of $\lambda = 0.1542$ nm. All WAXD measurements were performed at room temperature. Small-angle X-ray scattering (SAXS) experiments were carried out using the SAXS instrument at the BL17B3 beamline of the National Synchrotron Radiation Research Center (NSRRC), Taiwan. The blending samples of 1 mm thickness in general were sealed between two thin Kapton windows (80 μm in thickness) and measured at room temperature. The FT-IR spectrum of the KBr disk was measured using a Nicolet Avatar 320 FT-IR spectrometer, and 32 scans were collected at a resolution of 1 cm^{-1}. The DMF solution containing the sample was cast onto a KBr disk and dried under conditions similar to those used in the bulk preparation. The sample chamber was purged with nitrogen, and the KBr disk was heated to 120 °C to maintain film dryness.

Results and Discussion

Block Copolymer Analyses. PVPh and PCL-*b*-P4VP copolymers used in this work were respectively prepared by living anionic polymerization and through a subsequent hydrolysis reaction and by ring-opening polymerization followed by TEMPO as described elsewhere.[20−24] The GPC traces of PCL and PCL-*b*-P4VP block copolymer obtained after polymerization are shown in Figure 1, indicating that block copolymers prepared from the PCL macroinitiator resulted in high symmetry and were

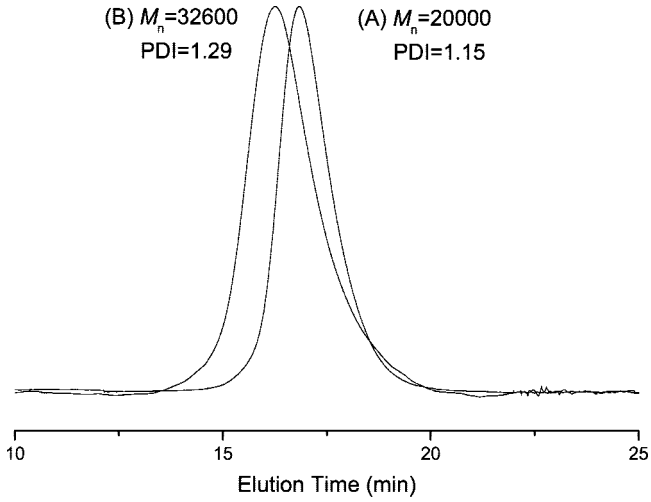

Figure 1. GPC traces of (A) poly(ε-caprolactone) ($M_w/M_n = 1.15$; $M_n = 20\,000$) and (B) the PCL-*b*-P4VP block copolymer ($M_w/M_n = 1.29$; $M_n = 32\,600$) in DMF.

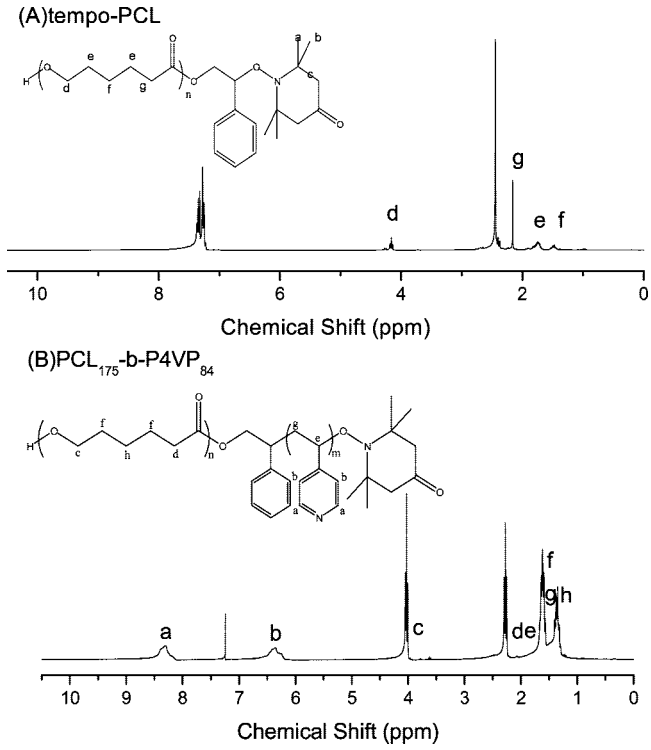

Figure 2. ^{1}H NMR spectra: (A) the PCL-TEMPO macroinitiator in $C_6D_5CD_3$; and (B) the PCL-*b*-P4VP block copolymer in $CDCl_3$.

monomodal (PDI = 1.15). The absence of the PCL macroinitiator peak and shift to lower retention time support the formation of PCL-*b*-P4VP block copolymers. The polydispersity of the block copolymer of ε-caprolactone and 4-vinylpyridine is ca. 1.29. Parts a and b of Figure 2 display the ^{1}H NMR spectra of the PCL-TEMPO macroinitiator and block copolymer. The latter spectrum features characteristic peaks of the resonances of both the PCL and the P4VP blocks. Table 1 summarizes molecular weights of the PVPh and PCL-*b*-P4VP copolymers employed in this study.

Block Copolymer/Homopolymer Analyses. *Thermal Analyses.* Figure 3 shows the conventional second run DSC thermograms of PCL-*b*-P4VP/PVPh blends in various compositions obtained by a heating rate of 20 °C/min. First, for pure PCL-*b*-P4VP block copolymers, there are two glass transition

Table 1. Characterization of PVPh and PCL-*b*-P4VP Copolymers

copolymer	PCL_n-*b*-$P4VP_m$[a]		M_n[b]	M_w/M_n[b]
CV1	175	84	28 800	1.25
CV2	175	118	32 600	1.29
CV3	88	91	20 000	1.31
CV4	88	146	25 000	1.33
PVPh			6100	1.10

[a] Obtained by ^{1}H NMR spectra, where *n* and *m* are repeat units of PCL and P4VP blocks. [b] Obtained by GPC trace with DMF eluent of 0.6 mL/min and PS-standard calibration.

temperatures (T_g) and a melting temperature (T_m) because of the immiscibility between PCL and P4VP segments. The T_g's of the PCL block, the P4VP block, and the PVPh homopolymer are, respectively, at ca. −60, 150, and 181 °C, and the T_m of the PCL block is at ca. 55 °C. It is also noted that the amorphous P4VP has a T_g of 150 °C, which is much higher than the melting point of PCL crystallites (i.e., hard confinement).[25−28] Consequently, a well-defined system with strong segregation limits (high $(\chi N)_{Tc}$ value) for polymer crystallization under vitrified nanoscale confinement is generated.[29−31] Table 2 summarizes the thermal properties of PCL-*b*-P4VP/PVPh blend based on DSC analyses. The T_g of P4VP block shifts toward a higher value, and the T_g of PCL block remains unchanged with PCL-*b*-P4VP block copolymers blending with 20−60 wt % PVPh. Therefore, we speculate that the added PVPh acts preferentially with P4VP through hydrogen-bonding interaction. Besides, the melting peak of the crystalline PCL disappears totally when the PVPh content reaches 80 wt %. Meanwhile, PCL-*b*-P4VP/PVPh blends have only one glass transition temperature, suggesting that these blends become miscible when the PVPh content is 80 wt %. Eventually, PVPh acts like a common solvent between PCL and P4VP and induces the blends to become total miscible (disorder structure).

The phase diagram of PCL-*b*-P4VP/PVPh blends is shown in Figure 4. The presence of PVPh is able to enhance the immiscible block copolymers of PCL and P4VP, and the miscibility window shifts to the P4VP-rich region due to the significant ΔK effect.[32] This result is also consistent with a previous Coleman et al. study on the prediction of different interassociation equilibrium constants (ΔK) of a ternary hydrogen-bonded polymer blend.[32,33] This result is similar to previous Pomposo et al. studies on the PVPh/PEMA/PMMA ternary hydrogen-bonded polymer blend, showing that the PVPh is miscible with other components with more than 65 wt % of the PVPh.[34] More importantly, we are interested in their morphological transformation of order structure in this immiscible block copolymer/homopolymer blend composition by TEM and SAXS analyses in the later sections.

TEM Analyses. Figure 5 illustrates the different types of self-assembly morphologies observed by TEM. After RuO_4 staining, the PVPh and P4VP microdomains are dark, and the PCL microdomains appear light. Clearly, Figure 5A and B represents the lamellar structures of CV1 and CV2 showing regular pattern with lamellar period of ca. 25−30 nm. Figure 5C presents the hexagonal PCL cylinders dispersed within the P4VP matrix in pure CV4. The average microdomain radius and the distance between spheres measured by TEM micrographs are ca. 20 and 30 nm, respectively. The morphological transformation can be observed from lamellar structure to hexagonal cylinder structure when CV1 and CV2 are blended with 20 wt % PVPh as shown in Figure 5D and E. According to Figure 5F (CV4/PVPh = 80/20 wt %), we can observe that a microdomain radius is ca. 15 nm and the distance between spheres is ca. 20 nm. This sphere structure as the dark region corresponds to a mixed phase of P4VP and PVPh; the bright region corresponds to the PCL phase that has been confined within the mixed phase because of its significantly weaker ability to form hydrogen bonds with

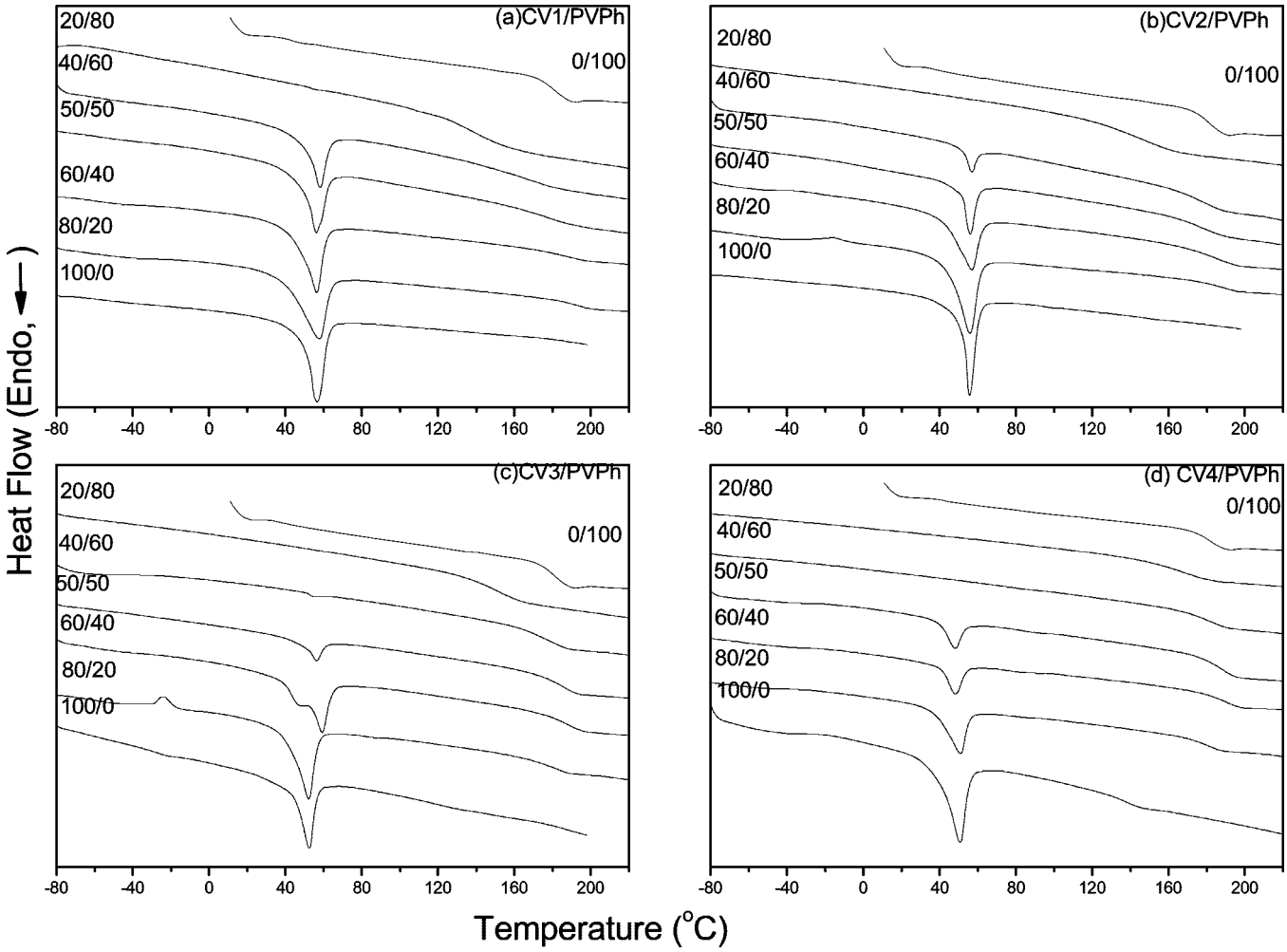

Figure 3. DSC thermograms of PCL-*b*-P4VP/PVPh blends, having different compositions for (a) CV1/PVPh, (b) CV2/PVPh, (c) CV3/PVPh, and (d) CV4/PVPh.

Table 2. Thermal Properties of PCL-*b*-P4VP/PVPh Blends

copolymer	PVPh content (wt %)	T_f (°C)	T_m (°C)	T_g (°C)
CV1	0	34.7	56.8	−52.0/151.0
	20	−46.1/33.1	57.5	−51.3/187.0
	40	−50.8/35.8	56.0	−52.1/190.0
	50	32.7	56.0	−49.1/178.8
	60	31.9	58.3	−49.0/173.0
	80			146.5
CV2	0	32.7	56.5	−56.4/150.0
	20	−49.6	55.9	−57.9/187.7
	40	32.7	56.6	−57.9/191.3
	50	33.5	55.9	−56.4/186.9
	60	30.7	56.6	−52.1/185.5
	80			154.3
CV3	0	20.4	52.2	−55.7/144.9
	20	−55.0	52.2	−55.0/182.6
	40	−50.0/31.0	46.7/59.4	−52.8/192.0
	50	31.0	56.6	−53.5/188.4
	60	31.0	54.4	181.8
	80			159.4
CV4	0	−49.9	50.1	−52.1/145.0
	20	−57.9	50.9	−55.0/182.5
	40	−45.9/−36.6	47.9	−54.3/192.8
	50	−47.4/−23.8	47.9	−51.3/189.9
	60			187.7
	80			172.3

PVPh. In other words, the crystalline PCL is restricted by the existing phase due to the vitrification of the amorphous phase. As we mentioned above, PCL is immiscible with P4VP, and the PCL-*b*-P4VP is a well-defined system with strong segregated

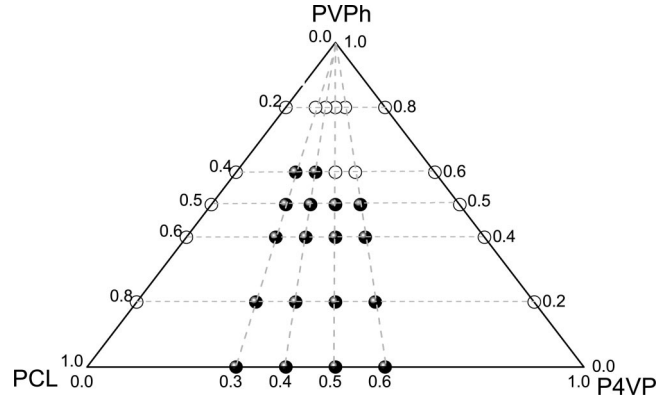

Figure 4. Block copolymer/homopolymer phase diagram of the PCL-*b*-P4VP/PVPh system. The "○" represent miscible, and the "●" represent immiscible.

microphase separation. The incorporation of PVPh in the PCL-*b*-P4VP system may increase the interaction parameter difference P4VP/PVPh and PCL phases because of the difference in interassociation equilibrium constants from PVPh/P4VP (K_A = 598) and PVPh/PCL (K_A = 90) phases. Therefore, PVPh forms hydrogen bonding with P4VP preferentially, and the T_g of P4VP/PVPh is substantially higher than the T_g of P4VP by blending the appropriate content of PVPh into PCL-*b*-P4VP copolymers. In other words, the P4VP/PVPh phase has greater ability to confine the PCL phase, and the original volume fraction of PCL

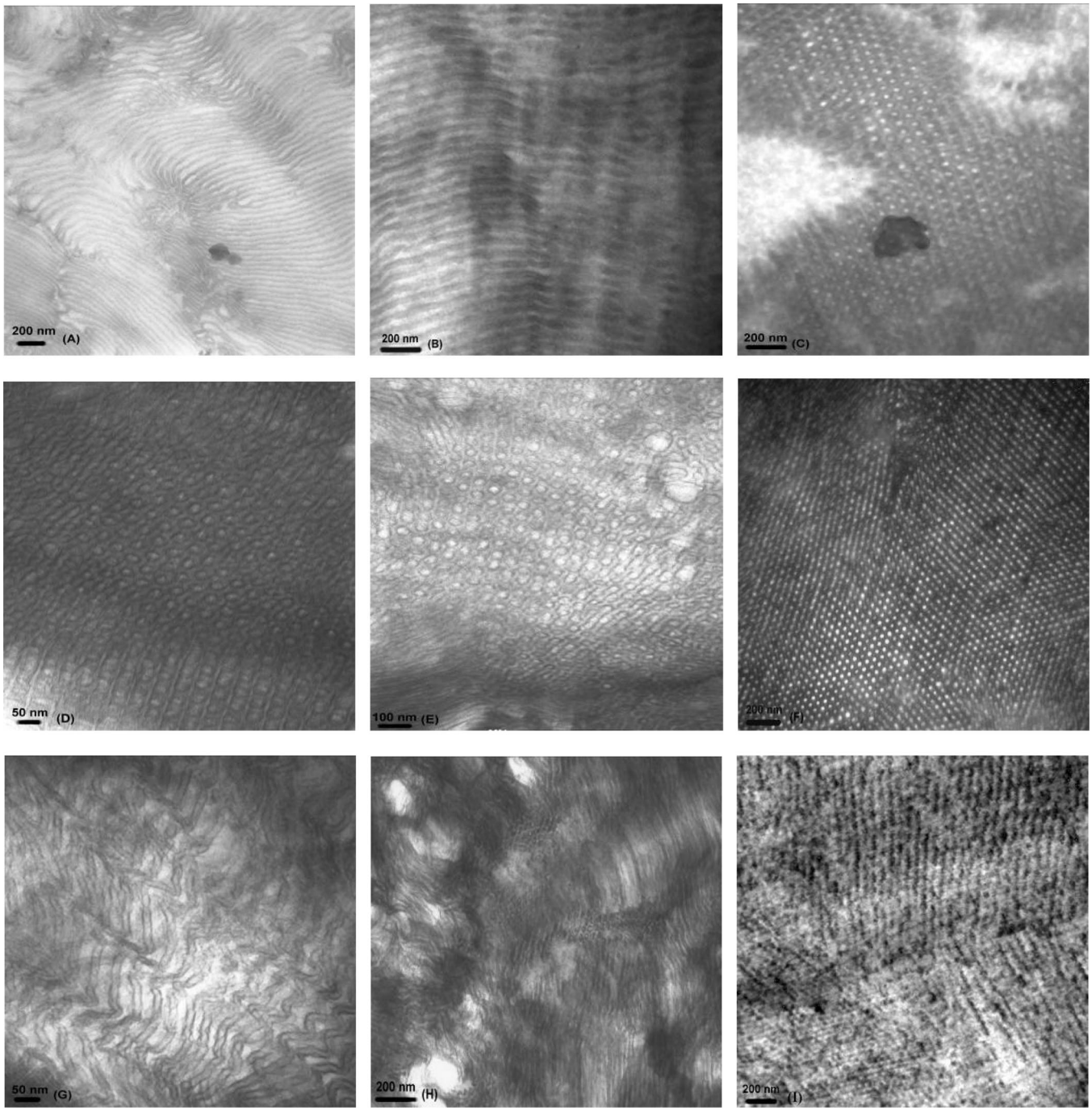

Figure 5. Transmission electron micrographs of the solution-cast films of (A) pure CV1, (B) pure CV2, (C) pure CV4, (D) CV1/PVPh = 80/20 wt %, (E) CV2/PVPh = 80/20 wt %, (F) CV4/PVPh = 80/20 wt %, (G) CV1/PVPh = 60/40 wt %, (H) CV2/PVPh = 60/40 wt %, and (I) CV4/PVPh = 60/40 wt % blend stained with RuO_4. (A) and (B) correspond to lamellar structures. (C), (D), and (E) represent hexagonal cylinder structures. (F) shows a more regular sphere structure. (G) represents a disordered lamellar structure. (H) and (I) show partial cylinder and partial lamellae.

may be changed. Next, the driving forces for this self-assembly structure are coming from not only the segregation interaction between PCL and P4VP but also different interassociation equilibrium constants from PVPh/P4VP and PVPh/PCL. Therefore, the CV4/PVPh = 80/20 wt % blend (Figure 5F) is able to form a more regular sphere structure. However, with further increase on PVPh content (>40 wt %), PVPh is also able to form hydrogen-bonding interaction with PCL, thus inducing the morphologies of these blends to become a wormlike structure.[14] The morphologies of different PCL-*b*-P4VP copolymers blending with 40 wt % PVPh are shown in Figure 5G−I. Obviously, the long-range order self-assembly structure becomes poor in the formation of wormlike or rodlike structure (partial cylinder and partial lamellae in the blends of CV2/PVPh = 60/40 and CV4/PVPh = 60/40 simultaneously). We speculate that the remnant PVPh interacts with the PCL phase through hydrogen bonding and induces the morphologies changing from ordered cylinder to coexistent cylinder and lamellae structure. Comparing CV1/PVPh = 60/40 to CV1/PVPh = 80/20, the morphology transforms directly into disordered lamellar structure as shown in Figure 5G. Eventually, the PVPh acts like a common solvent in the blend system, and the blend becomes miscible (disorder structure) when the PVPh content is above 60 wt %, which also coincide with results from DSC analyses.

SAXS Analyses. SAXS profiles of PCL-*b*-P4VP/PVPh blends are taken at room temperature to confirm the microphase-separated morphologies at room temperature and are shown in Figure 6. Pure CV4 block copolymer shows the first-order

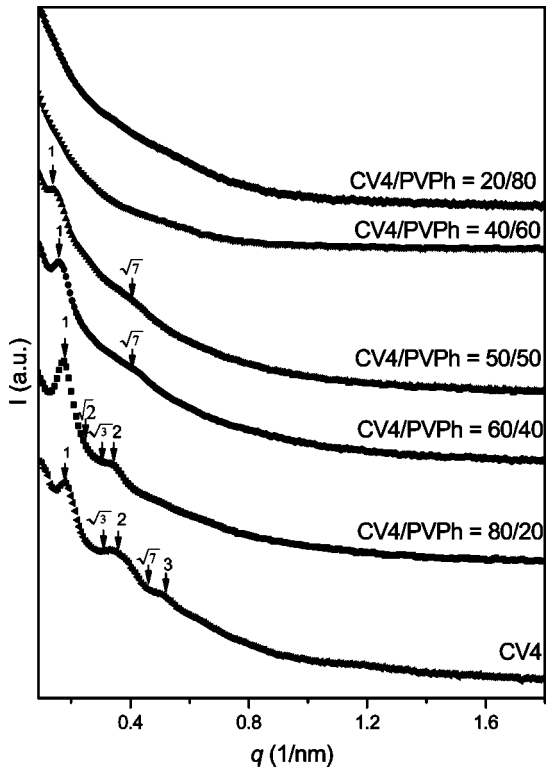

Figure 6. Profiles of Lorentz-corrected SAXS intensity of CV4/PVPh blends of different compositions.

scattering broad peak corresponding to a Bragg spacing of 34.0 nm, the average spacing between the PCL and neighboring P4VP microphases. Pure CV4 also shows long-range order structure with a ratio of peak positions of $1:\sqrt{3}:2$, revealing an ordered phase of hexagonally packed cylinders. The CV4/PVPh = 80/20 gives $1:\sqrt{2}:\sqrt{3}:2$ ratio positions, indicating a sphere structure. The blends at higher PVPh content (CV4/PVPh = 60/40 and 50/50 wt %) give broad peaks, indicating the absence of long-range ordered structure. However, both CV4/PVPh = 60/40 and 50/50 wt % show another small peak around $\sqrt{7}$ due to the incomplete disordering of the hexagonal cylinders present in these blends. The average spacing between the neighboring microdomains increases in the order of 35.8, 40.7, and 45.1 nm for 20, 40, and 50 wt % of PVPh content. Combining the TEM and SAXS results, we can conclude that there exists long-range order nanostructure in PCL-*b*-P4VP/PVPh at lower PVPh content (20 wt %), only short-range order nanostructure existed at relative higher PVPh content (40−60 wt %), and the disorder structure existed at the highest PVPh content (80 wt %).

FT-IR Analyses. As mentioned in DSC, SAXS, and TEM analyses, we know that the hydrogen-bonding strength of PVPh/P4VP is greater than that of the PVPh/PCL blend system. Further increasing the PVPh content, PVPh becomes available to interact with both P4VP and PCL through hydrogen bonding. By blending 80 wt % PVPh, the blends become miscible, and PVPh acts like a common solvent in this blend system. As a result, we will use the FTIR spectroscopy to provide this evidence.

Several regions within the infrared spectra of PCL-*b*-P4VP/PVPh blends are influenced by the hydrogen-bonding interaction. For convenience, only selected infrared spectra of CV4/PVPh blends are employed in this study. The hydroxyl stretching of various CV4/PVPh blends and pure PVPh cast from DMF solution at 120 °C (to eliminate the crystal effect of PCL block and the moisture absorption influence) is shown in Figure 7. Pure PVPh shows two unresolved bands in the hydroxyl stretching region, corresponding to the free hydroxyl at 3525 cm^{-1} and a very broadband centered at 3400 cm^{-1} from the absorption of hydrogen-bonded hydroxyl group (self-association) at 180 °C as shown in Figure 7a. The intensity of the free hydroxyl group increased gradually with the increase of the PVPh content in this blend system as would be expected. In addition, Figure 7a displays that the hydroxyl shifts into lower wavenumber when the P4VP is the rich content in the blend (lower PVPh content), implying that PVPh hydroxyl preferably interacts with the P4VP pyridine. Therefore, it is reasonable to assign the band at 3125 cm^{-1} to the hydrogen-bonded hydroxyl with pyridine because a relatively smaller number of the hydroxyl groups tends to interact completely with pyridine groups of P4VP block to form hydrogen bonding. Meanwhile, the peak frequency of the broadband shifts higher with increasing PVPh content, reflecting a new distribution of hydrogen-bonding formation resulting from the competition between the hydroxyl−hydroxyl group within the pure PVPh and hydroxyl−carbonyl group between PVPh and PCL (3430 cm^{-1}). Moskala and co-workers have used the frequency difference between the hydrogen-bonded hydroxyl absorption and the free absorption ($\Delta\upsilon$) to roughly estimate the average hydrogen-bonding strength.[35] In this respect, hydrogen-bonding interactions between PVPh hydroxyl and P4VP pyridine ($\Delta\upsilon$ = 400 cm^{-1}) are stronger than those between PVPh hydroxyl and PCL carbonyl ($\Delta\upsilon$ = 95 cm^{-1}), which is consistent with the prediction from the Painter−Coleman association model (PCAM). According to the PCAM, the interassociation equilibrium constant of the PVPh/P4VP blend (K_A = 598) is significantly greater than that of the PVPh/PCL blend (K_A = 90), implying that the hydrogen-bond formation between PVPh and P4VP predominates over that between PVPh and PCL in these PCL-*b*-P4VP/PVPh blends.

The carbonyl group of PCL blocks is sensitive to hydrogen-bonding interactions. The peaks at 1735 and 1710 cm^{-1} correspond to the free carbonyl and hydrogen-bonded carbonyl. Figure 7b presents FTIR spectra of the carbonyl stretching region, ranging from 1680 to 1780 cm^{-1}, of PCL-*b*-P4VP and PCL-*b*-P4VP/PVPh blends at 120 °C to eliminate the crystal effect of PCL block at 1724 cm^{-1}. The hydrogen-bonded carbonyl band of PCL at 1710 cm^{-1} starts to appear in these blends containing PVPh content above 40 wt %, indicating that the PVPh hydroxyl starts to interact with PCL carbonyl. As expected, a higher content of vinyl phenol units results in a higher number of hydrogen-bonded carbonyl groups. Besides, the band at 993 cm^{-1} also can be used to analyze the hydrogen-bonding interactions between the hydroxyl group of PVPh and the pyridine group of P4VP. Figure 7c shows the scale-expanded infrared spectra in the range 980−1020 cm^{-1} measured at 120 °C for PVPh, CV4, and CV4/PVPh blends. Pure CV4 has a characteristic band at 993 cm^{-1} corresponding to the pure pyridine ring absorption of P4VP block. Pure PVPh does not absorb at 993 cm^{-1} but has a band at 1013 cm^{-1}. These two bands are well resolved without overlapping. Upon hydrogen bonding between PVPh and P4VP, a new band at 1005 cm^{-1} is assigned to hydrogen-bonded pyridine rings.[15] It is difficult to calculate the quantitative fraction of hydrogen bonding due to the presence of three bands in this region. As a result, the digital subtraction of the pure PVPh peak at 1013 cm^{-1} based on its mole fraction of the PVPh in these blends system is carried out in this work. The Gaussian function has been used to curve fit the carbonyl stretching frequencies of PCL at 1735 and 1710 cm^{-1} and the pyridine bands of P4VP at 993 and 1005 cm^{-1}, corresponding to their respective free and hydrogen-bonded groups. To obtain the true fraction of the hydrogen-bonded group, a known absorptivity ratio for hydrogen-bonded and free group is required. Values of $\alpha_{HB}/\alpha_F = 1.5$ for carbonyl of PCL

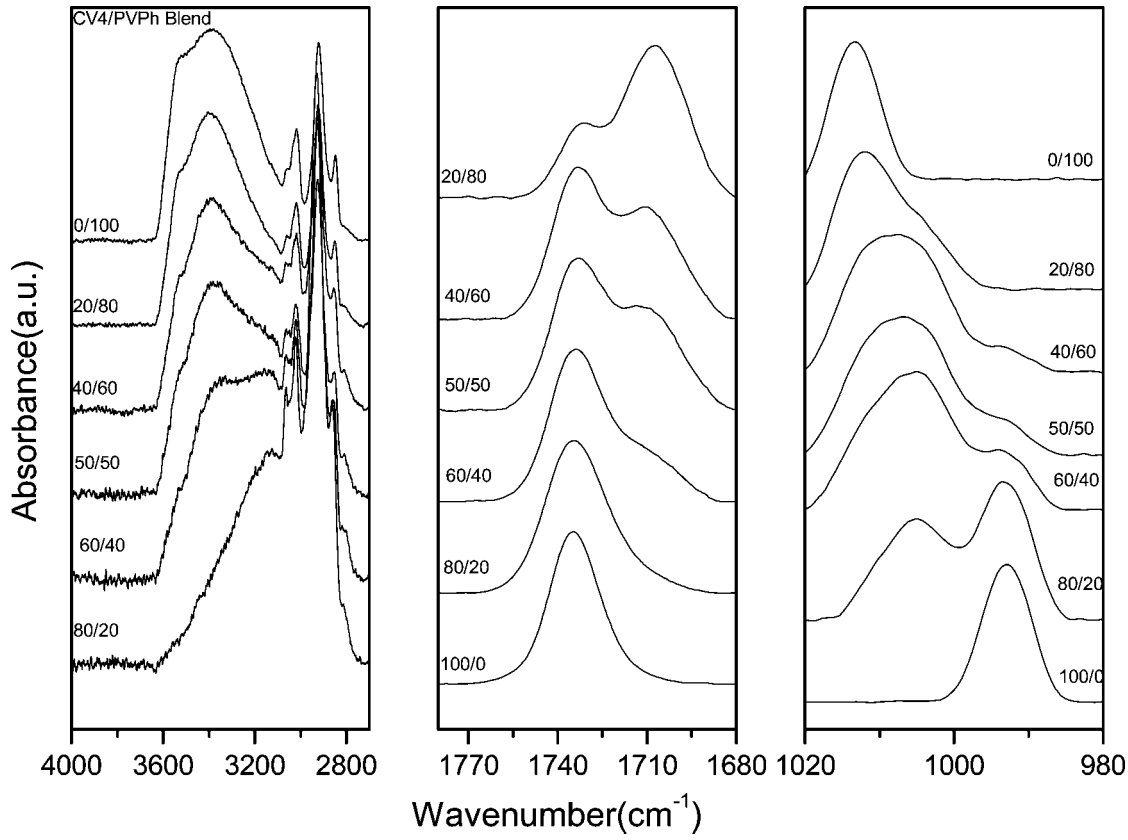

Figure 7. FT-IR spectra recorded at 120 °C displaying the (a) hydroxyl stretching, (b) carbonyl, and (c) pyridine region.

Table 3. Curve Fitting of Hydrogen-Bonded Carbonyl Groups and Pyridine Groups of CV4/PVPh Blends

CV4/PVPh	ν_f (cm^{-1})	A_f (%)	ν_b (cm^{-1})	A_b (%)	f_b[a]	ν_f (cm^{-1})	A_f (%)	ν_b (cm^{-1})	A_b (%)	f_b[a]
100/0	1735	100		0	0	993	100		0	0
80/20	1734	87.8	1711	12.2	8.5	993	50.4	1005	49.6	49.6
60/40	1734	72.1	1711	27.9	20.5	993	20.6	1005	79.4	79.4
50/50	1734	53.9	1710	46.1	36.3	993	13.8	1005	86.2	86.2
40/60	1734	50.2	1710	49.8	39.8	993	10.5	1005	89.5	89.5
20/80	1733	23.8	1709	76.2	68.1		0	1006	100	100

[a] f_b: fraction of hydrogen bonding.

Table 4. Summary of the Self- and Interassociation Equilibrium Constants and Their Thermodynamic Parameter of PCL-*b*-P4VP/PVPh Blends at 25 °C[a]

				equilibrium constant			enthalpy (kcal/mol)		
polymer	V	M_w	δ	K_2	K_B	K_A	h_2	h_B	h_A
PVPh	100	120	10.60	21.0	66.8		−5.6	−5.2	
P4VP	84.9	105.1	10.85			598			−7.0
PCL	107	114	9.21			90			−4.3

[a] V: molar volume (mL/mol). M_w: molecular weight (g/mol). δ: solubility parameter (cal/mL)$^{1/2}$. K_2: dimer self-association equilibrium constant. K_B: multimer self-association equilibrium constant. K_A: interassociation equilibrium constant. h_2: enthalpy of dimer self-association formation. h_B: enthalpy of multimer self-association formation. h_A: enthalpy of interassociation formation.

and 1 for pyridine of P4VP are employed.[18,36] Table 3 summarizes the curve-fitting results of CV4/PVPh blends in terms of the fraction of hydrogen-bonded carbonyl and pyridine. It is clear that the PVPh hydroxyl is able to form hydrogen bonds with both P4VP and PCL when the PVPh content is above 40 wt %. In other words, hydroxyl groups of PVPh form hydrogen bonds only preferentially with pyridine of P4VP when PVPh content is below 40 wt %.

According to the Painter−Coleman association model (PCAM),[18,19,37−40] we designate B, A, and C as PVPh, PCL, and P4VP, respectively, and K_2, K_B, K_A, and K_C as their corresponding association equilibrium constants. The self-association constants of PVPh ($K_2 = 21.0$ and $K_B = 66.8$) and the interassociation constant between PVPh and P4VP ($K_C = 598$) have been determined.[18] The interassociation constant K_A value is determined directly from a least-squares fitting procedure based on the fraction of hydrogen-bonded carbonyl experimentally obtained in the binary PVPh/PCL blend ($K_A = 90$).[16,17] Table 4 lists all of the parameters required by the Painter−Coleman association model to estimate thermodynamic properties for these blends. Figure 8 plots the experimental data and the prediction curves by using the PCAM model of PCL-*b*-P4VP/PVPh versus PVPh weight fraction of these four blend systems from the FT-IR of hydrogen-bonded carbonyl and pyridine region. It is worth noting that there is a large negative deviation of PCL hydrogen-bonded carbonyl group, but it gives a positive deviation of P4VP hydrogen-bonded pyridine group from the PCAM prediction curve ($K_A = 90$, $h_A = -4.0$ kcal/mol, $K_C = 598$, $h_C = -7.0$ kcal/mol). Clearly, with an increase in the composition of P4VP in block copolymers, the larger

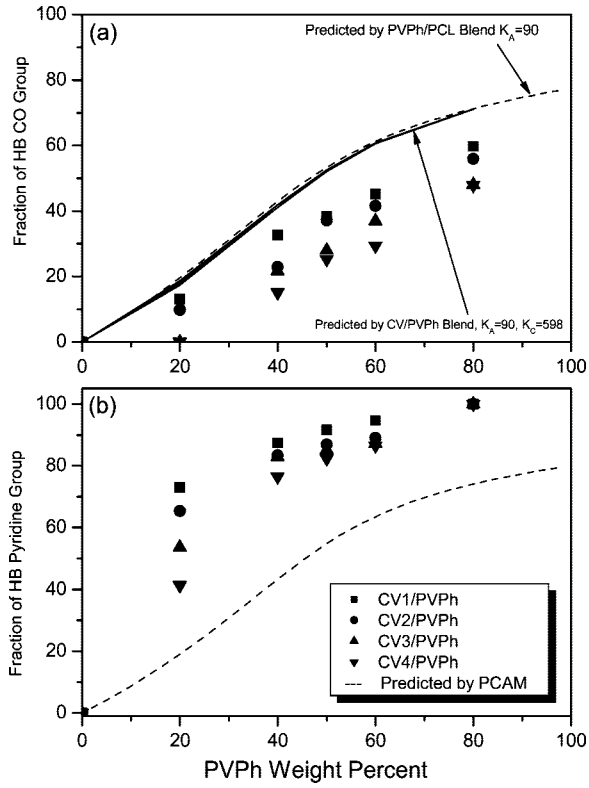

Figure 8. Experimental data of (a) hydrogen-bonded carbonyl group and (b) hydrogen-bonded pyridine group with PCAM prediction.

negative deviation from experiment and prediction data was found in hydrogen-bonded carbonyl group, but gives only a relatively smaller deviation in hydrogen-bonded pyridine group. The main reason for such a deviation is that the interassociation equilibrium constant of PVPh/P4VP is significantly greater than that of PVPh/PCL; thus the PCL tends to be excluded from the PVPh/P4VP phase as shown in Figures 5 and 6. The microphase separation of PCL block decreases the intermolecular hydrogen-bonding interaction between PVPh and PCL; as a result, the experimental data of the hydrogen-bonded carbonyl group are lower than the predicted data. On the contrary, it enhances the intermolecular hydrogen-bonding interaction between PVPh and P4VP; thus the experimental data are higher than the predicted data.

In summary, Figure 9 plots the T_g of the PVPh/P4VP phase versus PVPh/PCL ratio. At lower PVPh/PCL ratio (<0.7), the T_g behavior of PVPh/P4VP blend increases significantly with the increase of PVPh content and shows the long-range order self-assembly structure (cylinder or sphere). Most hydroxyl groups of PVPh are preferably interacted with pyridine groups of P4VP, resulting in relatively lower hydrogen-bonded carbonyl groups of PCL (0−0.13) than the predicted value by PCAM, and the PCL phase is excluded from the PVPh/P4VP phase to form more regular microphase separation structure. With the increase of PVPh/PCL ratio (0.7−3), the T_g of PVPh/P4VP starts to decrease with the increase of PVPh content because the hydroxyl group of PVPh becomes available to interact with the carbonyl group of PCL ($f_b^{C=O} = 0.15-0.45$) and thus destroys the long-range order self-assembly structure of PCL phase and transforms into short-range order wormlike structure. With further increase of PVPh/PCL ratio (>3.0), the T_g of PVPh/P4VP decreases significantly with the increase of the PVPh content, and the PCL-*b*-P4VP/PVPh blend becomes the disorder miscible phase, as more hydroxyl groups of PVPh interact with the carbonyl group of PCL ($f_b^{C=O} = 0.48-0.6$), and the crystal structure of PCL totally disappeared. Scheme 2 summarizes the

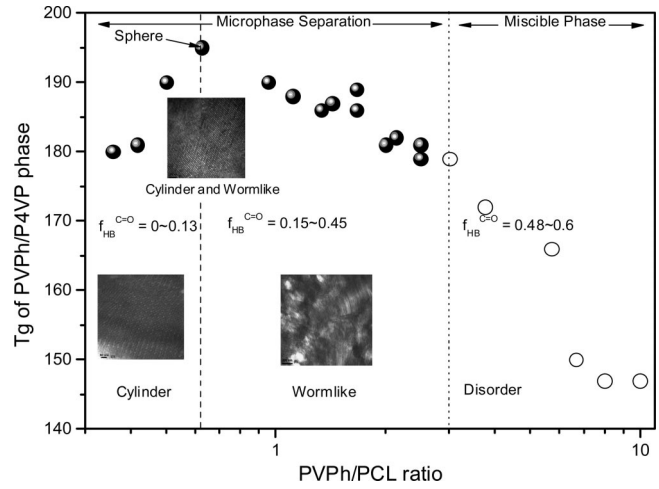

Figure 9. T_g behavior of PVPh/P4VP phase versus PVPh/PCL ratio in PCL-*b*-P4VP/PVPh blend.

detailed morphology change with the increase of PVPh content in this PCL-*b*-P4VP/PVPh blend system.

Crystallization Behavior. In previous study of Guo et al.[13,14] on the blending of PCL-*b*-P2VP/PVPh, the melting temperature of PCL decreases with the increase of PVPh contents. In addition, the T_g of PVPh/P2VP is located between two pure homopolymers. However, the PCL melting temperature does not change and even increases with the increase of PVPh contents in this PCL-*b*-P4VP/PVPh system, while the T_g of PVPh/P4VP is significantly higher than both pure homopolymers as shown in Table 2. The main difference in procedure employed is the high cooling rate (20 °C/min) in the PCL-*b*-P2VP/PVPh blend, and thus the regular self-assembly structures (hard confinements of PCL) cannot be obtained. Figure 10 shows the DSC cooling curves of PCL-*b*-P4VP/PVPh blends obtained at a fixed cooling rate of 5 °C/min. Table 2 also summarizes the freezing temperatures of PCL-*b*-P4VP/PVPh blends based on Figure 10. The peak temperature of the crystallization exotherm is defined as freezing temperature (T_f), where a higher T_f corresponds to a faster crystallization rate. Many previous works have reported that the freezing temperature (T_f) associates with the nonisothermal crystallization under a fixed cooling rate and displays a distinct correlation with the microdomain structure.[41−47]

Clearly, a single exotherm was found at lower PVPh content (0−20 wt %). However, a peculiar crystallization behavior (two exotherms) was found with the increase of PVPh content; the second exotherm II at lower T_f, not present in the PCL homopolymer, appears at much larger undercooling. Because of lower PCL content such as pure CV4 and CV4/PVPh = 80/20, PCL will form a regular disperse phase as shown in Figure 5C and F, whose average size is so small that the number of particles is much greater than the number of active heterogeneities usually present in this polymer, which is called hard confinement and only shows one exotherm. By further increase of PVPh content (>40 wt %), PVPh will start to interact with PCL based on FTIR analyses, so the self-assembly will change to short-range order structure because of PCL confinement destroying. Crystallization may take place with more than one exotherm, and that is precisely termed "fractionated crystallization".[48,49] In addition, this copolymer/homopolymer blend shows only one melting temperature in Figure 3, which is understood by considering that the first crystallization process (exotherm I) is produced by heterogeneous crystallization (continuous domains, in which case crystal growth can propagate throughout the sample as shown in Figure 5G−I) and the second exotherm by homogeneous nucleation (independent (noncon-

Scheme 2. Morphology Change in PCL-*b*-P4VP/PVPh Blends with the Increase of PVPh Contents

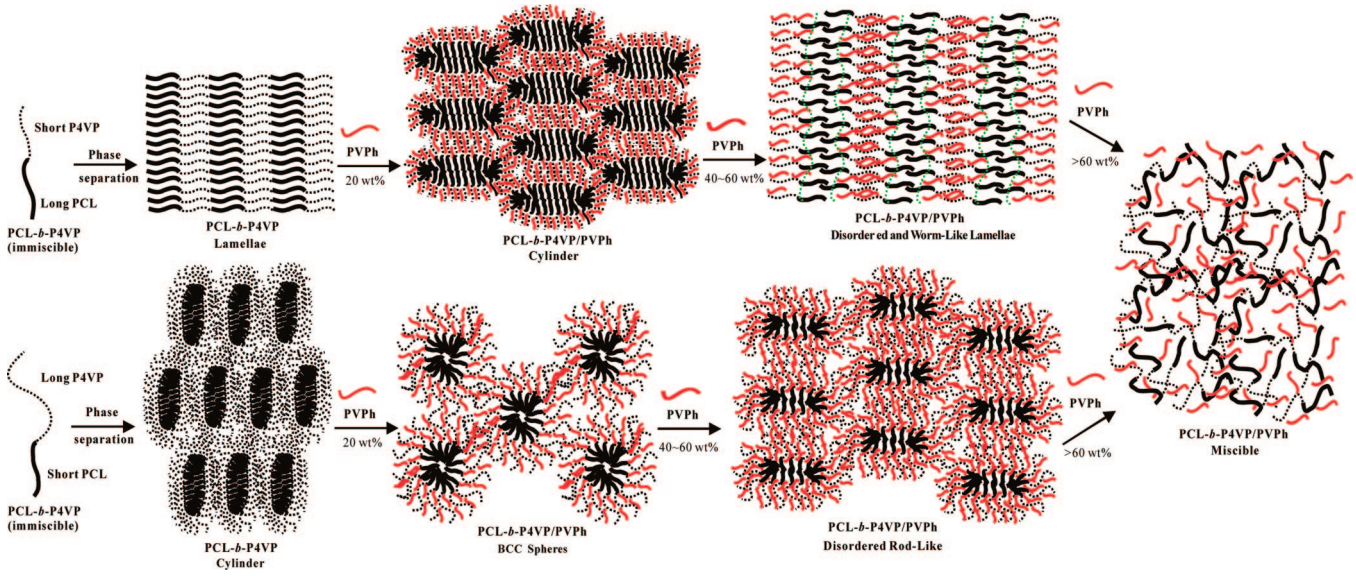

necting) PCL domains in PVPh/PVP mixed phase) as shown in Figure 5C and F. A similar phenomenon has been reported by Chen et al.[41,42] They reported the strongly segregated diblock systems under a fixed cooling rate; the freezing temperature associated with nonisothermal crystallization displayed a distinct correlation with the microdomain structure. T_f dropped abruptly as the melt morphology changed from extended lamellae to dispersed cylinders. A second drop of T_f was observed as the

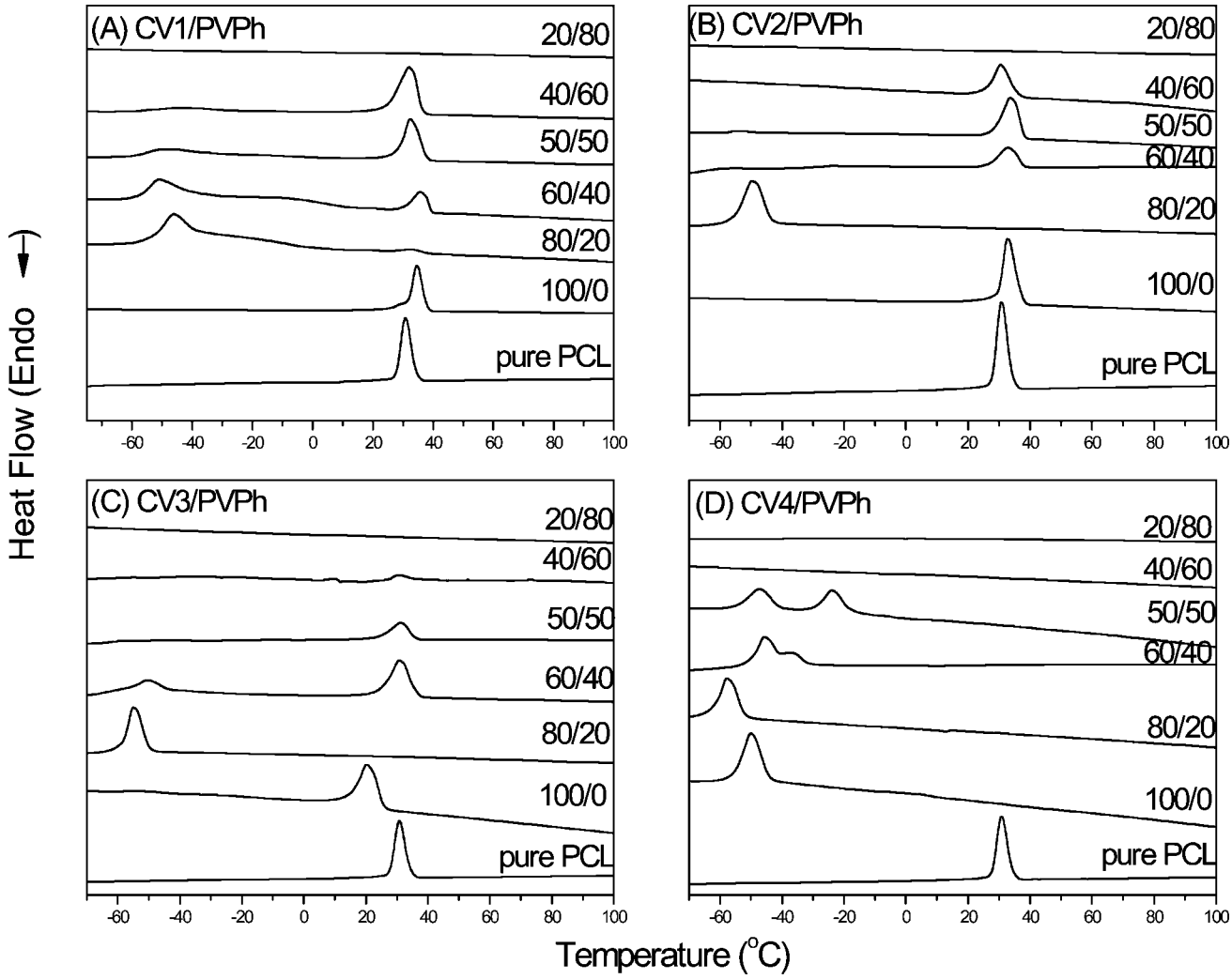

Figure 10. DSC cooling curves of PCL-*b*-P4VP/PVPh blends for (a) CV1/PVPh, (b) CV2/PVPh, (c) CV3/PVPh, and (d) CV4/PVPh with a constant cooling rate of 5 °C/min.

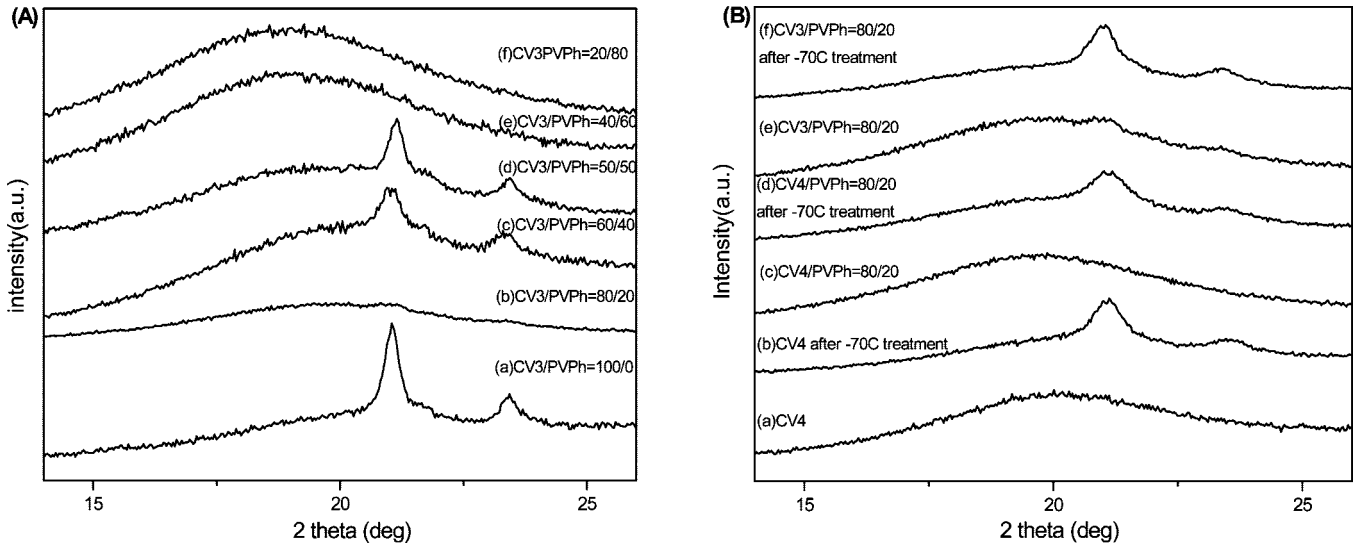

Figure 11. WAXD patterns of (A) pure CV3 and CV3/PVPh blends of different compositions, and (B) CV3/PVPh = 80/20, CV4/PVPh = 80/20 wt %, and pure CV4.

morphology further transformed into spheres. The degree of supercooling ($\Delta T = T_m^0 - T_f$, $T_m^0 = 75$ °C)[50] required to initiate crystallization in the lamellar microdomains (ΔT = 50 °C) is comparable to that associated with the PCL homopolymer (ΔT = 42 °C); exceedingly large undercoolings are required for crystallizations in cylindrical (ΔT = 125 °C). The crystallization kinetics exhibits distinct transitions at the compositions corresponding to the morphological transformation, which demonstrates the feasibility of exploiting microdomain pattern by manipulating the crystallization kinetics of the block chains. As shown in Figure 10, pure CV1, CV2, and CV3 show the freezing temperature at ca. 20−35 °C; as a result, we would expect the lamellar structure in these pure diblock copolymers as shown in Figure 5A and B. However, pure CV4 shows the freezing temperature at −50 °C that should correspond to the cylinder structure as shown in Figure 5C. Clearly, the freezing temperatures decrease significantly at 20 wt % of PVPh content in all PCL-*b*-P4VP copolymers. The freezing temperatures decrease with the decreasing of PCL content in PCL-*b*-P4VP diblock copolymers at PCL-*b*-P4VP/PVPh = 80/20 (more confinement) as shown in Table 2. Because of the changes of the freezing temperatures (from lamellae (T_f = 20−35 °C) to cylinder (T_f = −50 to −55 °C)), we can expect that the CV1, CV2, and CV3 blending with 20 wt % of PVPh content should give the cylinder structure.

In other words, the self-assembly morphology of PCL-*b*-P4VP can be transferred by blending with 20 wt % PVPh because the added PVPh preferentially forms hydrogen bonding with P4VP block and the PCL block is confined with the PVPh/P4VP phase. However, the crystalline PCL is destroyed, and no crystallization exotherm is observed with 80 wt % PVPh. As a result, the PVPh content in the blends plays an important role in affecting the crystallization behavior and the morphological changes because of the nanostructural confinement.[41] Further evidence for the exotherm II is the corresponding homogeneous nucleation at ca. −50 °C, by using wide-angle X-ray diffraction. The XRD data of PCL-*b*-PVPh/PVP blends are shown in Figure 11.

Figure 11 shows the WAXD data of PCL-*b*-P4VP/PVPh blends for different compositions and treatments at room temperature. The crystalline PCL shows two distinct diffraction peaks for all blends at 2θ = 21.5° and 23.8° as (110) and (200) reflections, corresponding to the orthorhombic packing as a perfect crystallographic orientation of the crystalline structures of the pure PCL.[47,51] The diffraction peaks of crystalline PCL appears as shown in part (a) of Figure 11A because the PCL block is immiscible with the P4VP block and thus forms the crystalline structure. It is worth mentioning that the crystallization peak disappears by blending 20 wt % PVPh with CV3 but appears again by blending 40−50 wt % PVPh as shown in Figure 11A. Further increasing the PVPh content to 60−80 wt %, the crystallization peak disappears again and results in amorphous halos in the WAXD because a large number of hydroxyl groups of PVPh form hydrogen bonding with the pyridine groups of P4VP and carbonyl groups of PCL. In other words, the blend becomes miscible, and the crystalline structure of the PCL is destroyed. However, this result is in contrast to the DSC analysis as show in Figure 3, showing that this composition PCL-*b*-P4VP/PVPh = 80/20 wt % blend has a strong melting peak of the crystalline PCL. In general, the polymer crystallinity measured by WAXD is from in situ measurement, and no thermal history is involved in preparing the sample. On the contrary, the polymer crystallinity detected by DSC depends on the thermal history because recrystallization may occur during the cooling or heating scan. According to the DSC results (Figure 10), we can conclude that the pure CV4 and some compositions of PCL-*b*-P4VP/PVPh blends require certain degrees of supercooling to initiate crystallization of PCL. As a result, these samples need to cool below −50 °C to initiate the crystallization of PCL as shown in Figure 11. Figure 11 illustrates that the crystal diffraction peaks of these samples are observed after −70 °C treatment, which are also in good agreement with DSC analyses.

Conclusions

DSC, WAXD, TEM, SAXS, and FT-IR techniques have been employed to investigate in detail the miscibility, phase behavior, and hydrogen-bonding interaction mechanism of this novel A−B/C type polymer blend composed of immiscible PCL-*b*-P4VP and PVPh. Results from DSC demonstrate that PVPh preferentially forms hydrogen bonding with P4VP block; the original T_g of P4VP shifts higher, while the T_g of PCL remains unchanged by blending with 20−50 wt % PVPh. Meanwhile, these compositions of blends are immiscible because of the presence of two T_g and one T_m. Further increasing the PVPh content, abundant PVPh becomes available to interact with both P4VP and PCL through hydrogen bonding. By blending 80 wt % PVPh, the blends become miscible, and PVPh acts like a common solvent in this blend system. Moreover, the cooling results of DSC show that the structure transition of PCL occurred

through the T_f of PCL changing. WAXD results are also in a good agreement with the cooling results of DSC. TEM images and SAXS analyses indicate that different compositions of PCL-*b*-P4VP/PVPh blends result in different microphase-separated structures through the mediation of hydrogen-bonding interactions even though PCL-*b*-P4VP is immiscible. FT-IR spectra also provide evidence that the P4VP pyridine group is a significantly stronger hydrogen-bond acceptor than the PCL carbonyl group and that PVPh interacts with P4VP preferentially through stronger hydrogen-bonding interactions in PCL-*b*-P4VP/PVPh blends. In this way, we can obtain different self-assembly morphologies in PCL-*b*-P4VP/PVPh blends with the increase of PVPh contents.

Acknowledgment. This work was supported financially by the National Science Council of the ROC under contracts NSC-96-2120-M-009-009 and NSC-96-2218-E-110-008 and the Ministry of Education "Aim for the top University" (MOEATU) program. The SAXS experiments were conducted at beamline BL17B3 at the National Synchrotron Radiation Research Center (NSRRC), Taiwan.

References and Notes

(1) Rodriguez-Hernandez, J.; Checot, F.; Gnanou, Y.; Lecommandoux, S. *Prog. Polym. Sci.* **2005**, *30*, 691.
(2) Hamley, I. U. *The Physics of Block Copolymers*; Oxford University Press: Oxford, UK, 1998.
(3) Foerster, S.; Antonietti, M. *Adv. Mater.* **1998**, *10*, 195.
(4) Hadjichristidis, N.; Pispas, S.; Floudas, G. A. *Block Copolymers Synthetic Strategies, Physical Properties, and Applications*; John Wiley & Sons: Hoboken, 2003.
(5) Han, Y. K.; Pearce, E. M.; Kwei, T. K. *Macromolecules* **2000**, *33*, 1321.
(6) Zhao, J. Q.; Pearce, E. M.; Kwei, T. K. *Macromolecules* **1997**, *30*, 7119.
(7) Bendejacq, D.; Ponsinet, V.; Joanicot, M. *Macromolecules* **2002**, *35*, 6645.
(8) Zoelen, W. V.; Ekenstein, G. A.; Ikkala, O.; ten-Brinke, G. *Macromolecules* **2006**, *39*, 574.
(9) Huang, P.; Zhu, L.; Cheng, S. Z. D.; Ge, Q.; Quirk, R. P.; Thomas, E. L.; Lotz, B.; Hsiao, B. S.; Liu, L. Z.; Yeh, F. J. *Macromolecules* **2001**, *34*, 649.
(10) Jinnai, H.; Hasegawa, H.; Nishikawa, Y.; Sevink, G. J.; Braunfeld, M. B.; Agard, D. A.; Spontak, R. J. *Macromol. Rapid Commun.* **2006**, *27*, 1424.
(11) Dobrosielska, K.; Wakao, S.; Takano, A.; Matsushita, Y. *Macromolecules* **2008**, *41*, 7695.
(12) Kosonen, H.; Ruokolainen, J.; Nyholm, P.; Ikkala, O. *Polymer* **2001**, *42*, 9481.
(13) Hameed, N.; Guo, Q. *Polymer* **2008**, *49*, 922.
(14) Hameed, N.; Guo, Q. *Macromolecules* **2008**, *41*, 7596.
(15) Kuo, S. W.; Tung, P. H.; Chang, F. C. *Macromolecules* **2006**, *39*, 9388.
(16) Kuo, S. W.; Huang, C. F.; Lu, C. H.; Chang, F. C. *Macromol. Chem. Phys.* **2006**, *207*, 2006.
(17) Kuo, S. W.; Chan, S. C.; Chang, F. C. *Macromolecules* **2003**, *36*, 6653.
(18) Coleman, M. M.; Graf, J. F.; Painter, P. C. *Specific Interactions and the Miscibility of Polymer Blends*; Technomic Publishing: Lancaster, PA, 1991.
(19) Coleman, M. M.; Painter, P. C. *Miscible Polymer Blend-Background and Guide for Calculations and Design*; DEStech Publications, Inc., **2006**.
(20) Lin, C. L.; Chen, W. C.; Liao, C. S.; Su, Y. C.; Huang, C. F.; Kuo, S. W.; Chang, F. C. *Macromolecules* **2005**, *38*, 6435.
(21) Lu, C. H.; Huang, C. F.; Kuo, S. W.; Chang, F. C. *Macromolecules* **2009**, *42*, 1067.
(22) Chen, W. C.; Kuo, S. W.; Jeng, U. S.; Chang, F. C. *Macromolecules* **2008**, *41*, 1401.
(23) Tung, P. H.; Kuo, S. W.; Chang, F. C. *Polymer* **2007**, *48*, 3192.
(24) Chan, S. C.; Kuo, S. W.; Lu, C. H.; Lee, H. F.; Chang, F. C. *Polymer* **2007**, *48*, 5059.
(25) Huang, P.; Zhu, L.; Gau, Y.; Ge, Q.; Jing, A. J.; Chen, W. Y.; Quirk, R. P.; Cheng, S. Z. D.; Thomas, E. L.; Lotz, B.; Hsiao, B. S.; Avilaorta, C. A.; Sics, I. *Macromolecules* **2004**, *37*, 3689.
(26) Zhu, L.; Cheng, S. Z. D.; Callhoun, B. H.; Ge, Q.; Quirk, R. P.; Thomas, E. L.; Lotz, B.; Hsiao, B. S.; Yeh, F.; Liu, L. *Macromolecules* **2001**, *34*, 1244.
(27) Zhu, L.; Cheng, S. Z. D.; Calhoun, B. H.; Ge, Q.; Quirk, R. P.; Thomas, E. L.; Hsiao, B. S.; Yeh, F.; Lotz, B. *J. Am. Chem. Soc.* **2000**, *122*, 5957.
(28) Zhu, L.; Cheng, S. Z. D.; Hunag, P.; Ge, Q.; Quirk, R. P.; Thomas, E. L.; Lotz, B.; Hsiao, B. S.; Yeh, F.; Liu, L. *Adv. Mater.* **2002**, *14*, 31.
(29) Matsen, M. W.; Bates, F. S. *Macromolecules* **1996**, *29*, 1091.
(30) Semenov, A. N. *Sov. Phys. JEPT* **1985**, *61*, 733.
(31) Sun, Y. S.; Chung, T. M.; Li, Y. J.; Ho, R. M.; Ko, B. T.; Jeng, U. S.; Lotz, B. *Macromolecules* **2006**, *39*, 5782.
(32) Coleman, M. M.; Painter, P. C. *Prog. Polym. Sci.* **1995**, *20*, 1.
(33) Manestrel, C. L.; Bhagwagar, D. E.; Painter, P. C.; Coleman, M. M.; Graf, J. F. *Macromolecules* **1992**, *25*, 7101.
(34) Pomposo, J. A.; Calahorra, E.; Eguiazabal, I.; Cortazar, M. *Macromolecules* **1993**, *26*, 2104.
(35) Moskala, E. J.; Varnell, D. F.; Coleman, M. M. *Polymer* **1985**, *26*, 228.
(36) Cesteros, L. C.; Meaurio, E.; Katime, I. *Macromolecules* **1993**, *26*, 2323.
(37) Kuo, S. W.; Chang, F. C. *Macromolecules* **2002**, *35*, 278.
(38) Kuo, S. W.; Chan, S. C.; Wu, H. D.; Chang, F. C. *Macromolecules* **2005**, *38*, 4729.
(39) Huang, C. F.; Kuo, S. W.; Lin, F. J.; Huang, W. J.; Wang, C. F.; Chang, F. C. *Macromolecules* **2006**, *39*, 300.
(40) Yen, Y. J.; Kuo, S. W.; Chang, F. C. *J. Phys. Chem. B* **2008**, *112*, 10821.
(41) Chen, H. L.; Hsiao, S. C.; Lin, T. L.; Yamauchi, K.; Hasegawa, H.; Hashimoto, T. *Macromolecules* **2001**, *34*, 671.
(42) Chen, H. L.; Wu, J. C.; Lin, T. L.; Lin, J. S. *Macromolecules* **2001**, *34*, 6936.
(43) Loo, Y. L.; Register, R. A.; Ryan, A. J.; Dee, G. T. *Macromolecules* **2001**, *34*, 8968.
(44) Chen, H. L.; Lin, S. Y.; Huang, Y. Y.; Chiu, F. C.; Liou, W.; Lin, J. S. *Macromolecules* **2002**, *35*, 9434.
(45) Xu, J. T.; Turners, S. C.; Fairclough, J. P. A.; Mai, S. M.; Ryan, A. J.; Chaibundit, C.; Booth, C. *Macromolecules* **2002**, *35*, 3614.
(46) Hsu, J. Y.; Hsieh, I. F.; Nandan, B.; Chiu, F. C.; Chen, J. H.; Jeng, U. S.; Chen, H. L. *Macromolecules* **2007**, *40*, 5014.
(47) He, C. L.; Sun, J. R.; Deng, M. X.; Chen, X. S.; Jing, X. B. *Biomacromolecules* **2004**, *5*, 2042.
(48) Balsamo, V.; von Gyldenfeldt, F.; Stadler, R. *Macromolecules* **1999**, *32*, 1226.
(49) Balsamo, V.; von Gyldenfeldt, F.; Stadler, R. *Macromol. Chem. Phys.* **1996**, *197*, 3317.
(50) Sun, J.; Chen, X.; He, C.; Jing, X. *Macromolecules* **2006**, *39*, 3717.
(51) Kuo, S. W.; Chang, F. C. *Macromol. Chem. Phys.* **2001**, *202*, 3112.

MA900080V